



# Digital-to-Analog Conversion of Pulse Amplitude Modulated Systems Using Adaptive Quantization

GIRIDHAR D. MANDYAM

*Nokia Research Center, 6000 Connection Drive, Irving, TX 75039, U.S.A.*

*E-mail: giridhar.mandyam@nokia.com*

**Abstract.** In this paper, a full analysis is presented on digital-to-analog conversion for pulse amplitude modulated (PAM) systems. By analyzing the cyclostationary nature of pulse-amplitude modulation (PAM) systems, two methods of quantization are proposed – fixed and adaptive. Examples of this quantization analysis are provided for the reverse link transmitter chain in a cdma2000 system, and for the baseband transmitter chain of an IS-136 system. In addition, the impact of D/A converter nonlinearity on resultant signal-to-noise ratio is analyzed. Simulations are provided which show that adaptive quantization provides performance benefits over fixed methods in terms of adjacent channel power rejection (ACPR) and transmitter signal-to-noise ratio.

**Keywords:** pulse-amplitude modulation, digital-to-analog conversion, transceivers.

## 1. Introduction

Pulse-amplitude modulation (PAM) is a common transmission method used for digital communications. PAM systems operate by passing information-bearing pulses through pulse-shaping filters to provide signals that are smoothed in time but band-limited in frequency. As a result, PAM transmission methods are often employed in wireless communications systems, which are bandlimited in nature.

PAM signals possess cyclostationary characteristics [1]. This property of PAM signals may be exploited in performing digital-to-analog conversion. In particular, one is interested in the scaling of the PAM signal prior to digital-to-analog conversion. Normally this scaling is a function of the probability density function of the signal. In this work, the PAM probability density function (pdf) is derived with respect to typical digital pulse-shaping. As examples, the cdma2000 and IS-136 systems are considered for analysis of pdf-optimized quantization with respect to cyclostationarity.

Similar to the IS-95-B system, the cdma2000 system [2] specifies the use of channel aggregation on the reverse link. However, a feature of cdma2000 channel aggregation not present in IS-95-B is the use of individual channel gain adjustment. These channel gain adjustments provide enhanced performance for coherent reverse link reception and can be used for quality-of-service considerations for data services. However, channel gains result in power adjustment of incoming data, which combined with pulse shaping, can dramatically affect resultant signal power. As a result, the effective spurious free dynamic range (SFDR) may degrade if quantization effects due to digital-to-analog conversion are not taken into account [3, 4]. In this paper, the D/A conversion issues for cdma2000 are analyzed, and quantization algorithms for scaling prior to the D/A converter are derived and simulated.

In addition, the IS-136 system [5] time-division multiple-access (TDMA) system also employs pulse-amplitude modulation. This type of system is just as sensitive to the dynamic

range of transceivers as the cdma2000 system. In this paper, the D/A conversion issues for the uplink baseband IS-136 subsystem are analyzed, with quantization algorithms derived and simulated in the same fashion as the cdma2000 systems.

## 2. Pulse-Amplitude Modulated Systems

Pulse amplitude-modulated (PAM) systems involve the transmission of pulse-shaped impulses. The amplitude of the impulses directly relates to the information that they are carrying. In general, a PAM signal may be expressed by the following expression [6]

$$y(t) = \sum_{n=-\infty}^{\infty} c_n p(t - nT), \quad (1)$$

where  $c_n$  represents the amplitude of the  $n$ th impulse, and  $p(t)$  is the pulse-shaping waveform.

In many modern digital radio systems, pulse-shaping is performed digitally. Two important reasons for this are: (A) it is often easier to implement the desired pulse waveform digitally than in the analog domain and (B) the pulse-shaping operation may be used to increase the sampling rate. Reason (A) relates to several aspects of the pulse-shaping filter, including matched filtering at the receiver and spectral shaping for electromagnetic compatibility. Reason (B) relates directly to the D/A conversion process, where sampling frequency affects the ease of design of not only the converter but also the sampling image-rejection filter that normally follows the DAC.

Of particular interest are the statistical properties of the PAM signal prior to D/A conversion. If one can fully characterize the PAM signal statistics, one may design an optimal quantizer for the signal. This leads directly to minimizing the distortion introduced by the D/A conversion process.

Assume that the series of impulses may be represented in the discrete-time domain by the signal  $x(n)$ , which is the amplitude of the impulse at the discrete-time index  $n$ . If we assume that the pulse-shaping filter  $N$ -tap  $h(n)$  has a tap-spacing of  $1/L$  times the time-interval between impulses and that  $x(n)$  is 0 for  $n < 0$ , then a version of  $x(n)$  must be created by zero-insertion:

$$x_e(n) = \sum_{k=-\infty}^{\infty} x(k)\delta(n - kL). \quad (2)$$

This process of zero-insertion introduces spectral copies of the original signal  $x(n)$  [9]; the ensuing pulse-shaping takes care of this and also introduces the desired pulse waveform. The final pulse-shaped waveform may be represented by the following relationship:

$$\begin{aligned} y(n) &= h(n) * x_e(n) \\ &= \sum_{r=0}^{N-1} h(r)x_e(n - r) \\ &= \sum_{k=0}^{\infty} \sum_{r=0}^{N-1} h(r)x(k)\delta(n - r - kL). \end{aligned} \quad (3)$$

This relationship may be simplified further by assuming that the pulse-shaping filter  $h(n)$  has length  $N$ , and that  $N$  is an integer multiple of  $L$ :

$$y(a + cL) = \sum_{r=0}^{\frac{N}{L}-1} h(rL + a)x(c - r), \quad (4)$$

where  $a$  is an integer such that  $0 \leq a < L$  and  $c$  is an integer such that  $c \geq 0$ . As is the case with PAM systems, it may be assumed that the signal  $x(n)$  is drawn from a finite length alphabet  $\{a_i\}$  of length  $A$ . If the alphabet is uniformly distributed, the probability density function of  $x(n)$  may be represented as

$$p_x(x) = \sum_{i=0}^{A-1} \frac{1}{A} \delta(x - a_i). \quad (5)$$

In (5),  $\delta(\cdot)$  is the dirac-delta function. Even if the alphabet is not uniformly distributed, it can be assumed that the signal  $x(n)$  is stationary, as its pdf does not vary in time. As can be seen by (4), the filtered-output signal  $y(n_0)$  at time  $n_0$  is dependent on  $N/L$  consecutive values of the stationary random process  $x(n)$  and the  $N/L$  coefficients drawn from  $h(n_0)$  to determine this value. Thus the pdf of  $y(n)$  may be expressed as

$$p_{y(a+cL)} = f\left(\sum_{r=0}^{\frac{N}{L}-1} h(rL + a)x(c - r)\right) = p_{y(a+dL)} \forall d, c, \quad (6)$$

where  $f(\cdot)$  is the pdf of its argument, and  $d$  is an integer such that  $d \geq 0$ . This relationship demonstrates the cyclostationary nature of  $y(n)$ .

One may narrow the assumption on the structure of  $h(n)$  to being *linear phase*. Therefore, these filter coefficients are symmetric, i.e.  $h(r) = h(N - r - 1)$  for  $0 \leq r < N$ . Referring to (4), one may group each set of  $N/L$  coefficients into subsets of  $h(r)$ :

$$h^i = \{h(i), h(L + i), \dots, h((N/L - 1)L + i)\} \quad 0 \leq i < L. \quad (7)$$

Taking advantage of the symmetry of the linear phase filter, one may rewrite each subset as

$$h^i = \left\{ \begin{array}{l} h(N - 1 - i), h(N - 1 - (L + i)), \dots, \\ h(N - 1 - ((N/L - 1)L + i)) \end{array} \right\} \quad 0 \leq i < L. \quad (8)$$

This in turn may be rewritten as

$$h^i = \left\{ \begin{array}{l} h((N/L - 1)L + L - 1 - i), h((N/L - 2)L + L - 1 - i), \dots, \\ h(L - 1 - i) \end{array} \right\} \quad (9)$$

$$0 \leq i < L.$$

The expression of  $h^i$  given in (9) is merely an order-reversal of  $h^{L-i-1}$ . As a result, the pdf's resulting from these two subsets should be equivalent. This may be seen from modifying (6):

$$\begin{aligned}
 p_{y(a+cL)} &= f \left( \sum_{r=0}^{\frac{N}{L}-1} h(rL+a)x(c-r) \right) = f \left( \sum_{r=0}^{\frac{N}{L}-1} h(N-1-(rL+a))x(c-r) \right) \\
 &= f \left( \sum_{r=0}^{\frac{N}{L}-1} h((N/L-r)L-a-1)x(c-r) \right) \\
 &= f \left( \sum_{r=0}^{\frac{N}{L}-1} h(rL+L-a-1)x(c-N/L+1+r) \right).
 \end{aligned} \tag{10}$$

Taking into account the stationarity of  $x(n)$ , then the following relationship holds:

$$\begin{aligned}
 &f \left( \sum_{r=0}^{\frac{N}{L}-1} h(rL+L-a-1)x(c-N/L+1+r) \right) \\
 &= f \left( \sum_{r=0}^{\frac{N}{L}-1} h(rL+L-a-1)x(c-r) \right) = p_{y(L-1+cL)}.
 \end{aligned} \tag{11}$$

Therefore, the number of pdf's associated with the filter  $h(n)$  of length  $N$  is

$$\text{ceil}(L/2), \tag{12}$$

where  $\text{ceil}(arg)$  is the smallest integer greater than or equal to  $arg$ . It can be seen that any D/A conversion method following the pulse-shaping operation needs to be optimized with respect to the pdf of the signal  $y(n)$ , and that if the pulse-shaping filter is linear phase, the number of individual pdf's associated with  $y(n)$  is equal to at least half of the oversampling ratio  $L$ , if in fact the length of the filter  $N$  is an integer multiple of  $L$ . *It is of interest to note that the problem of nonstationarity could be remedied by using a "stairstep"-shaped filter. Given the oversampling factor for the filter,  $L$ , and a filter length  $N = R \times L$ , the requirement for the causal form of such a filter would be:*

$$\begin{aligned}
 h(n) &= h(n+1) = h(n+2) = \dots = h(n+L-1) \\
 n &= 0, L, 2L, \dots, R \times L.
 \end{aligned} \tag{13}$$

If the pulse-shaping filter  $h(n)$  is linear-phase and has length  $N$ , and  $N$  is not an integer multiple of  $L$ , then the number of pdf's associated with the filter may not satisfy  $\text{ceil}(L/2)$ . For such a case, a filter that is linear phase may not produce the redundant pdf's that were demonstrated in the relationships of (10) and (11). Assume that  $N = \text{floor}(N/L) + R$ , where

$\text{floor}(arg)$  is the largest integer less than or equal to  $arg$ , and  $R$  is an integer such that  $0 < R \leq L - 1$ . The relationship of (4) must be modified:

$$\begin{aligned}
 y(a + cL) &= \sum_{r=0}^{\text{ceil}(\frac{N}{L})-1} h(rL + a)x(c - r), & 0 \leq a < R - 1 \\
 y(ak + cL) &= \sum_{r=0}^{\text{floor}(\frac{N}{L})-1} h(rL + a)x(c - r), & R \leq a < L.
 \end{aligned} \tag{14}$$

Each set of filter coefficients may now be grouped as:

$$\begin{aligned}
 h^i &= \{h(i), h(L + i), \dots, h((\text{ceil}(N/L) - 1)L + i)\}, & 0 \leq i < R - 1 \\
 h^i &= \{h(i), h(L + i), \dots, h((\text{floor}(N/L) - 1)L + i)\}, & R \leq i < L.
 \end{aligned} \tag{15}$$

Of the subsets given in by the relationship of (15), the subsets for  $h^i$  where  $0 < i < R - 1$  will have  $L + 1$  coefficients, while the remaining subsets will have  $L$  coefficients. One can clearly see that at least two pdf's will be evident in the output of the filter, as the filter coefficient subsets corresponding to each output will take one of two different lengths. The symmetry of (8) clearly does not hold for all filter coefficient subsets. In fact, the symmetry relationship of  $h^i$  with  $h^{L-i-1}$  as given by (9) will simply not hold when the length of  $h^i$  is not equal to  $h^{L-i-1}$ . First, let us examine the subsets given in (15) that correspond to  $0 \leq i < R - 1$ :

$$\begin{aligned}
 h^i &= \{h(i), h(L + i), \dots, h((\text{ceil}(N/L) - 1)L + i)\}, & 0 \leq i < R - 1 \\
 &= \{h(N - 1 - i), h(N - 1 - (L + i)), \dots, h(N - 1 - ((\text{ceil}(N/L) - 1)L + i))\} \\
 &= \left\{ \begin{array}{l} h((\text{ceil}(N/L) - 1)L + L - 1 - i - (L - R)), h((\text{ceil}(N/L) - 1)L + L - 1 - (L + i) - (L - R)), \\ \dots, h((\text{ceil}(N/L) - 1)L + L - 1 - ((\text{ceil}(N/L) - 1)L + i) - (L - R)) \end{array} \right\}
 \end{aligned} \tag{16}$$

(16) simplifies to

$$\begin{aligned}
 h^i &= \{h((\text{ceil}(N/L) - 1)L + R - 1 - i), h((\text{ceil}(N/L) - 1)L + R - 1 - i - L), \dots, h(R - 1 - i)\}, \\
 &0 \leq i < R - 1
 \end{aligned} \tag{17}$$

(17) is an order reversal of the  $(L + 1)$ -coefficient subset  $h^{R-1-i}$ , assuming such a distinct subset exists. Such symmetric subsets exist on if  $R - 1 > 0$ . Now, let us examine the subsets given in (15) that correspond to  $R \leq I < L$ :

$$\begin{aligned}
 h^i &= \{h(i), h(L + i), \dots, h((\text{floor}(N/L) - 1)L + i)\}, & R \leq i < L \\
 &= \{h(N - 1 - i), h(N - 1 - (L + i)), \dots, h(N - 1 - ((\text{floor}(N/L) - 1)L + i))\} \\
 &= \left\{ \begin{array}{l} h((\text{floor}(N/L) - 1)L + L - 1 - i + R), h((\text{floor}(N/L) - 1)L + L - 1 - (L + i) + R), \\ \dots, h((\text{floor}(N/L) - 1)L + L - 1 - ((\text{floor}(N/L) - 1)L + i) + R) \end{array} \right\}
 \end{aligned} \tag{18}$$

(18) simplifies to

$$\begin{aligned}
 h^i &= \{h((\text{floor}(N/L) - 1)L + L + R - 1 - i), h((\text{floor}(N/L) - 1)L + R - 1 - i), \dots, h(L + R - 1 - i)\}, \\
 &R \leq i < L
 \end{aligned} \tag{19}$$

(19) represents an order-reversal of the  $L$ -coefficient subset  $h^{L+R-1-i}$ , assuming such a distinct subset exists.

Such symmetric subsets only exist if  $L - 1 - R > 0$ . Therefore, the number of pdf's resulting from the filter output is

$$L - |R - \text{ceil}(L/2)|. \quad (20)$$

### 3. Optimal Quantization and Digital-to-Analog Conversion

Normally, in design of the baseband section of a PAM transmitter, the input to the digital-to-analog converter (DAC) is fixed-point. However, the number of bits occupied by the input to the DAC is typically much larger than the maximum number of bits that drive the DAC. In addition, the DAC translates equally-spaced input levels to equally-spaced output levels. Therefore, the collective process of scaling, truncation, and digital-to-analog conversion may be thought of as a uniform quantization procedure.

Assume the DAC takes as input zero-mean data, denoted by  $x$ . Given the DAC outputs  $L$  discrete levels spaced  $\Delta$  apart, the DAC output is taken from the discrete levels  $\{-(L-1)\Delta/2, \dots, -\Delta/2, \Delta/2, \dots, (L-1)\Delta/2\}$ . Assume that the input signal is divided into intervals as  $x \in \{(-\infty, -L\Delta/2], (-L\Delta/2, -(L+2)\Delta/2], \dots, ((L-2)\Delta/2, L\Delta/2], (L\Delta/2, \infty)\}$ . Thus each of the DAC output levels  $\{-(L-1)\Delta/2, \dots, -\Delta/2, \Delta/2, \dots, (L-1)\Delta/2\}$  corresponds to the input intervals  $\{(-L\Delta/2, -(L+2)\Delta/2], \dots, ((L-2)\Delta/2, L\Delta/2]\}$ . The DAC rail output levels,  $\{-(L-1)\Delta/2, (L-1)\Delta/2\}$ , correspond to the input intervals  $\{(-\infty, -L\Delta/2], (L\Delta/2, \infty)\}$ . Thus, if the time-varying symmetric pdf of input signal  $x$  is denoted by  $p_x(x, i)$ , and the pdf of  $i$  is denoted by  $p_i(i)$ , then the mean-squared error between the DAC output signal  $r$  and the original signal  $x$  may be found by the following equation:

$$E\{(r-x)^2\} = 2 \int_{-\infty}^{\infty} \left[ \sum_{k=1}^{\frac{L}{2}-1} \int_{(k-1)\Delta}^{k\Delta} \left(x - \frac{(2k-1)\Delta}{2}\right)^2 p_x(x, i) dx + \int_{\frac{L\Delta}{2}}^{\infty} \left(x - \frac{(L-1)\Delta}{2}\right)^2 p_x(x, i) dx \right] p_i(i) \cdot \quad (21)$$

If  $x$  is a PAM signal, then the function  $p_x(x, i)$  is not continuous over  $i$  due to its cyclostationary nature. Therefore, the mean-squared error derivation of (21) cannot be evaluated using a Riemann integral over a continuous function. Thus, one cannot find an optimal quantizer in the Lloyd-Max sense [7] for the output of this filter. However, due to the fact that the signal to be quantized in this case is cyclostationary, the integral may be evaluated as piecewise continuous. If the function  $p_x(x, i)$  is in fact cyclostationary with period  $T$ , then it will satisfy the relationship  $p_x(x, i) = p_x(x, i + NT)$ , where  $N$  is an integer. Moreover, assume that the function  $p_x(x, i)$  changes  $k$  times over one period. In addition, assume one period may be broken down into the disjoint intervals  $\{(A_0, A_1), (A_1, A_2), \dots, (A_{k-1}, A_k)\}$ , where the following hold true: (1)  $A_0 < A_1 < \dots < A_k$  (2)  $A_k - A_0 = T$ , and (3)  $p_x(x, A_j) = p_x(x, A_j + \varepsilon)$  for  $0 \leq \varepsilon < A_{j+1} - A_j$  and integer value  $j$  satisfying  $0 \leq j < k$ . In this case, the pdf of  $i$  for  $p_x(x, i)$  may be written as

$$p(i) = \frac{1}{A_{j+1} - A_j}, \quad A_j \leq i < A_{j+1}. \quad (22)$$

Now, the relationship of (22) may be evaluated in a piecewise form. Let us assume  $N$  pdf's exist. If these pdf's are denoted as  $p_x(x, j)$  ( $1 \leq j \leq N$ ), then the mean-squared error may now be written as

$$E\{(r-x)^2\} = \sum_{j=1}^N \left[ \sum_{k=1}^{\frac{L}{2}-1} \int_{(k-1)\Delta}^{k\Delta} \left(x - \frac{(2k-1)\Delta}{2}\right)^2 p_x(x, j) dx + \int_{\frac{L\Delta}{2}}^{\infty} \left(x - \frac{(L-1)\Delta}{2}\right)^2 p_x(x, j) dx \right]. \quad (23)$$

Thus given  $\log_2 L$  bits available in the DAC, an optimal quantizer may be found by minimizing the mean-squared error given in (26). This can be accomplished by scaling the input signal  $x$ , which adjusts the signal variance with respect to the maximum output level of the DAC.

Although the scaling factor that results from the minimum mean-squared error may be found analytically, the pdf is often difficult to find in closed-form. Therefore for a PAM system, sample data may be passed through the baseband pulse-shaping filter, scaled, and quantized to find the optimal scaling factors.

Although an adaptive quantizer that changes with the changing pdf in time might seem to provide better performance, one may need to modify the typical digital-to-analog conversion process along with the changing quantization. This becomes necessary as a consequence of the fact that adapting the scaling prior to the DAC can result in spectral distortion. This is due to the scaling adaptation rate being at  $L$  times the symbol rate ( $L$  being the oversampling factor of the pulse-shaping filter); although the change in scaling may be slight, this could result in significant spectral growth. Therefore, it is desirable to adjust the quantizer over the time-varying pdf to account for this spectral distortion. In the ensuing sections where specific systems are analyzed, the effects of spectral distortion and methods to account for it are provided.

#### 4. Example: CDMA2000 Signal Modeling Prior to Digital-to-Analog Conversion

Code division multiple access (CDMA) systems are particularly challenging for transmitter design. In general, CDMA systems employ PAM modulation along with feedback power control systems, resulting in a transmitter requirement for a large range of linearity. This requirement becomes challenging in the CDMA reverse link (or uplink), as in general, handset transmitter design is also optimized for cost and power consumption. This restricts many approaches to increasing linearity in the CDMA transmitter. The cdma2000 system is an example of a public wireless CDMA system which requires a large range of transmitter linearity. The challenges in analyzing the cdma2000 reverse link (Figure 1) arise from the possibility of a large number of pulse-shaped physical channels being transmitted simultaneously, thus generating a PAM signal. In this case, a pilot channel, one or more supplemental channels, a fundamental channel, and a dedicated control channel could be transmitted at any given instant in time. An individual channel gain may be denoted as  $G_{chan}$ . The channel gains (relative to the pilot channel) of the supplemental, fundamental, and dedicated control channels are designated as  $G_s$ ,  $G_f$ , and  $G_c$ . The pilot channel gain,  $G_{PI}$ , is always one.

Assume that user data on any given channel after Walsh code and PN-code spreading is denoted by  $\{x_{chan}(k)\}$ , where  $k$  is the discrete time index for each chip.  $x_{chan}$  is uniformly distributed and taken from the alphabet  $\{-1, +1\}$ , the resultant variance of data is 1. Adjusting

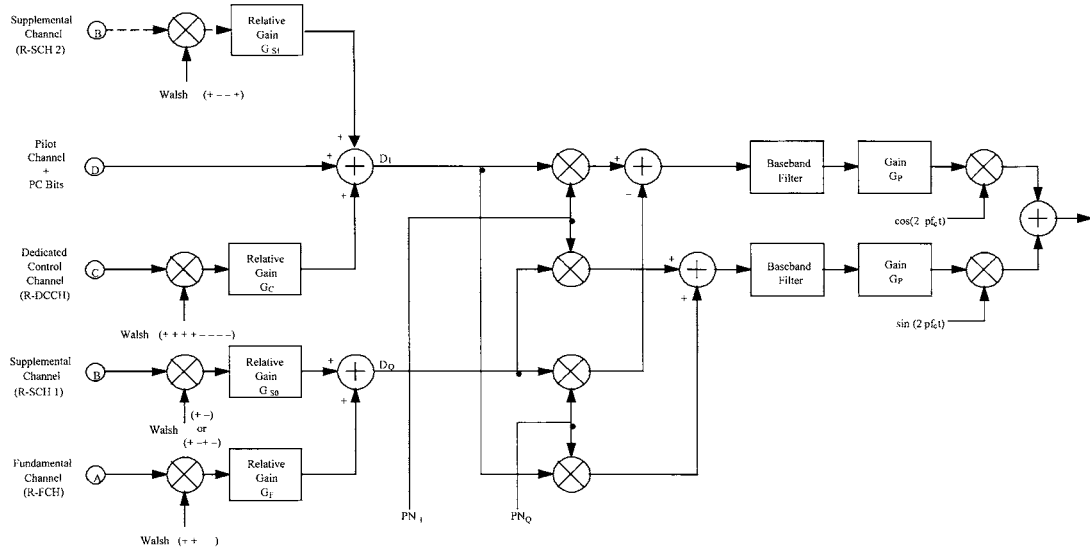


Figure 1. cdma2000 transmitter.

by the channel gain factor results in a variance of  $G_{chan}^2$ . However, the data is passed through a baseband pulse-shaping filter. This filter, whose tap spacing is  $1/4$  of a chip, is 48 taps long. If three zeros are inserted between each datum in  $\{x_{chan}(k)\}$ , then the resultant sequence may be denoted as  $\{d_{chan}(l)\}$ , where the following applies:

$$\{d_{chan}(l)\} = \{x_{chan}(0), 0, 0, 0, x_{chan}(1), 0, 0, 0, \dots\}. \quad (24)$$

The variance of this sequence is now one quarter of the variance of the original sequence, i.e.  $G_{chan}^2/4$ . After passing this sequence through the baseband pulse-shaping filter [8] (depicted in Figure 2, with a gain bias of 6 dB for display purposes), whose coefficients are denoted by  $\{h(r)\}$ , where  $0 \leq r < 48$ , the resultant signal,  $y_{chan}(l)$ , has the sample variance

$$\sigma_{y_{chan}}^2 = \frac{G_{chan}^2}{4} \sum_{r=0}^{47} h^2(r). \quad (25)$$

Assuming the data on one channel is uncorrelated with the data from another channel, the overall variance of the aggregate channels is

$$\begin{aligned} \sigma^2 &= \sigma_{y_s}^2 + \sigma_{y_f}^2 + \sigma_{y_s}^2 + \sigma_{y_{PI}}^2 \\ &= \frac{\sum_{r=0}^{47} h^2(r)}{4} (G_c^2 + G_f^2 + G_s^2 + G_{PI}^2) \\ &= \frac{\sum_{r=0}^{47} h^2(r)}{4} (G_c^2 + G_f^2 + G_s^2 + 1) \end{aligned} \quad (26)$$

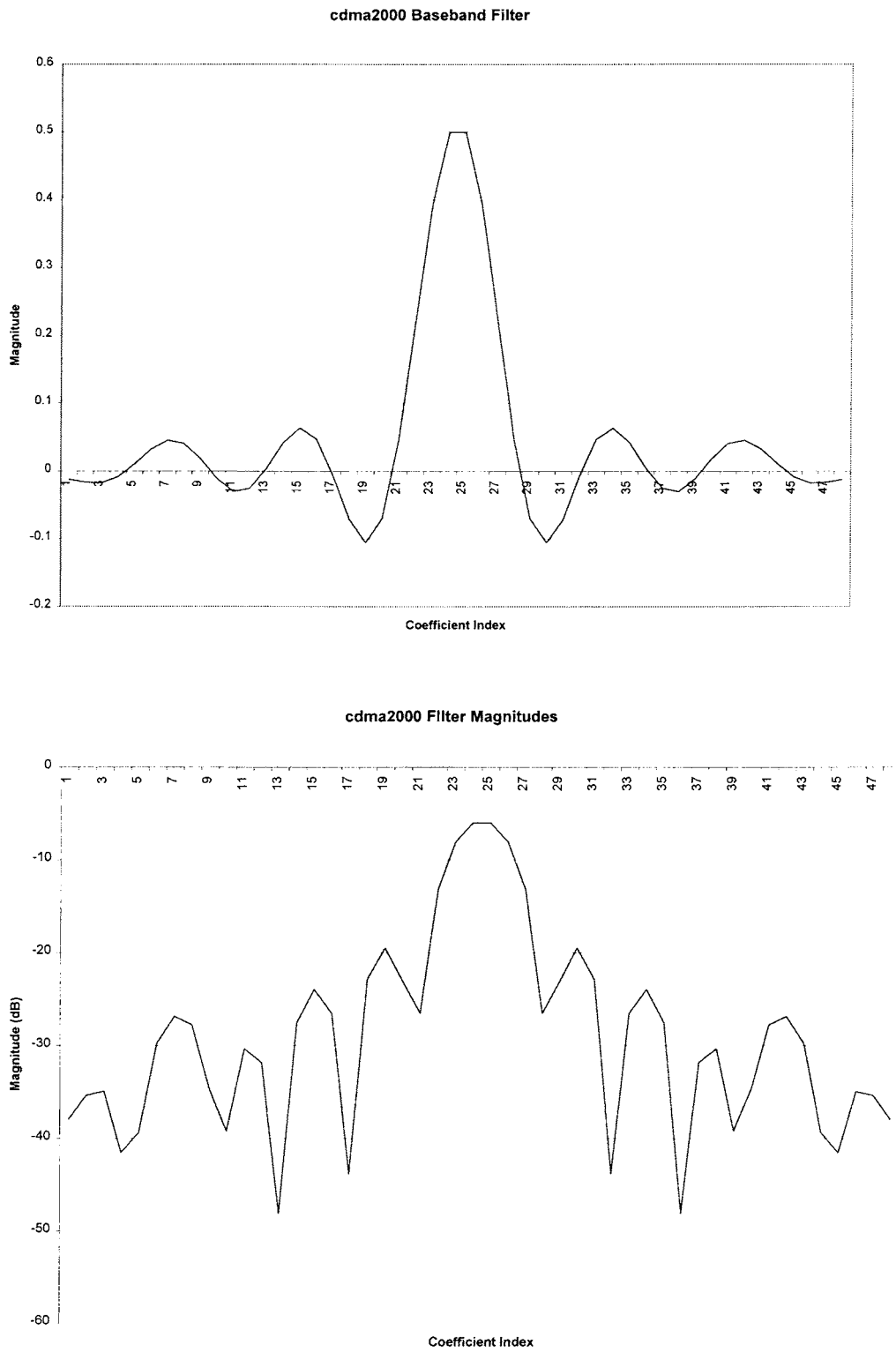


Figure 2. cdma2000 baseband filter.

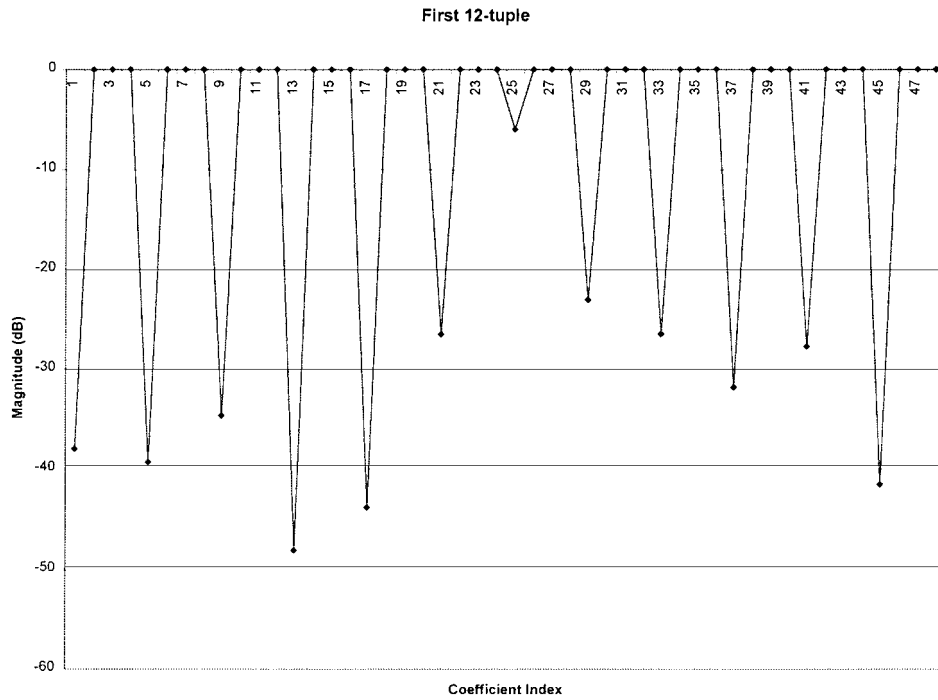


Figure 3. First 12-tuple of coefficients,  $h^1(r)$ .

$y_{chan}(l)$  is not Gaussian. This can be seen by referring to the convolution relationship that defines  $y_{chan}(l)$ :

$$y_{chan}(l) = \sum_{i=0}^{47} h(i)d_{chan}(l-i). \quad (27)$$

Although the convolution equation indicates that the calculation of  $y_{chan}(l)$  results from 48 multiplications and 47 additions; in fact, due to the zero insertion in  $d_{chan}(l)$ , the result actually comes about from 12 multiplications and 11 additions. Assuming that the filter coefficients may be represented by the corresponding 12-tuples, i.e.  $\{h(r)\} = \{h^1(r), h^2(r), h^3(r), h^4(r)\}$ , where  $h^i(r)$  is a group of 12 filter coefficients resulting in a single filter output, then by observing the gains resulting from multiplication from each group of 12 coefficients from  $h(r)$  (Figures 3–6), one can see that in two cases only one of the coefficients is dominant. Thus central limit theorem arguments for Gaussianity become ineffective.

A typical distribution of coefficients for one channel output based on the 12-tuple of Figure 3 is shown in Figure 7. As expected, since the convolution sum is basically dominated by one filter coefficient, the distribution resembles that of an antipodal signal in white noise. The “white noise” in this case is a result of the contributions of the smaller filter coefficients (“smaller” in this case means any coefficients other than the maximum gain coefficient in each 12-tuple of filter coefficients). As there is more than one smaller coefficient of similar gain value in this particular 12-tuple of filter coefficients, the central limit theorem argument is strengthened for the filter output due to one 12-tuple alone. This topic will be examined in more detail.

Due to the fact that the “dominant” coefficient changes in magnitude between each of the 12-tuples, the process resulting from the baseband filter is in fact cyclostationary. This can be

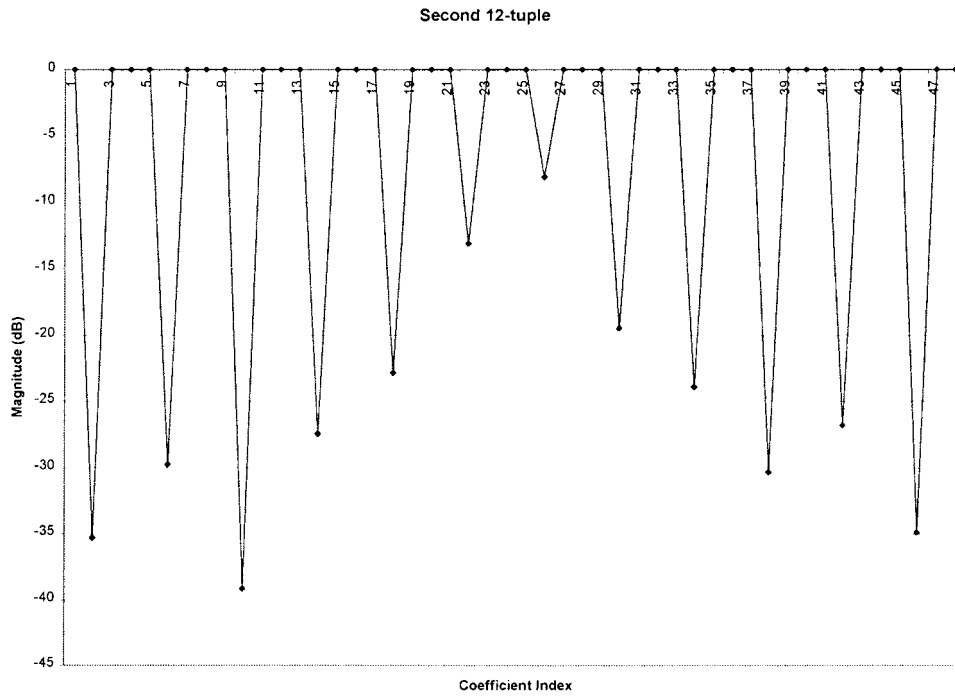


Figure 4. Second 12-tuple of coefficients,  $h^2(r)$ .

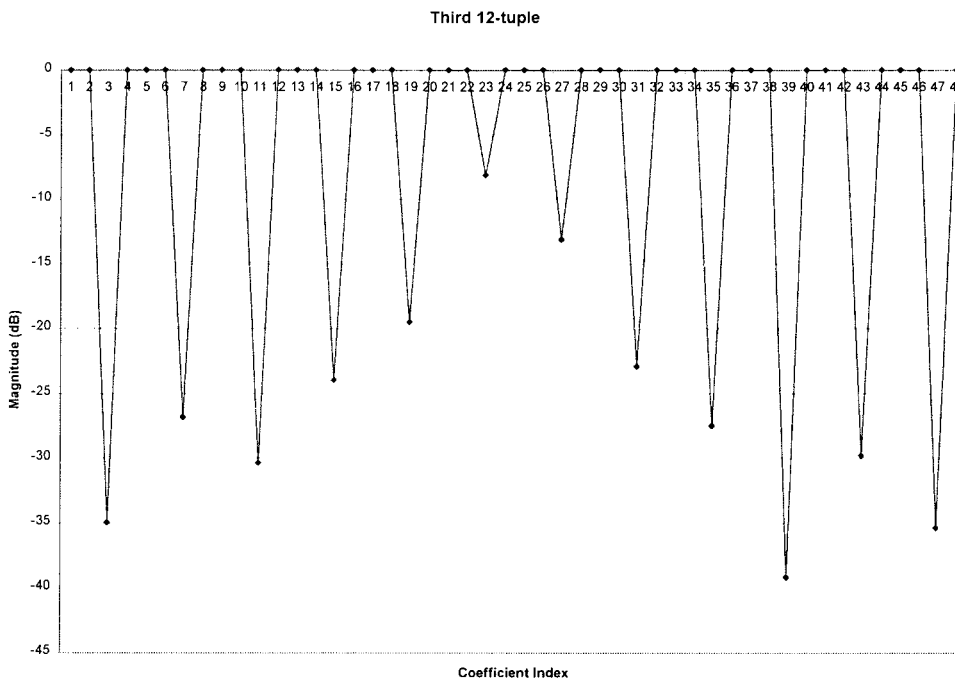


Figure 5. Third 12-tuple of coefficients,  $h^3(r)$ .

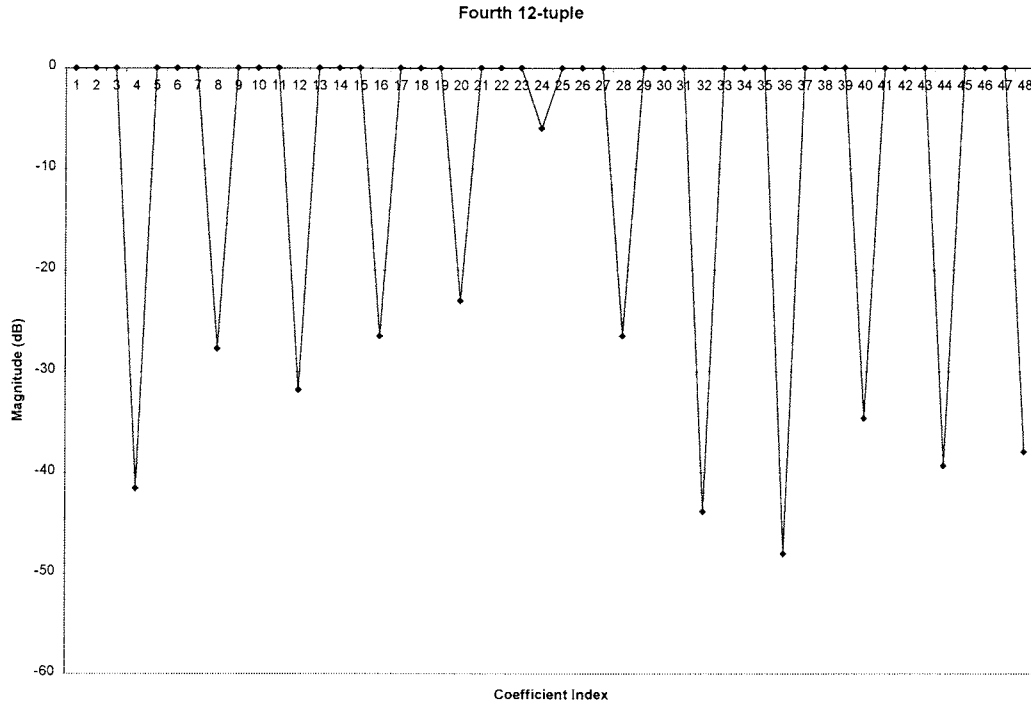


Figure 6. Fourth 12-tuple of coefficients,  $h^4(r)$ .

seen from the 12-tuple gains depicted in Figures 3–6. As can be seen, the peak gain factors are clearly not the same for each 12-tuple, and the smaller gain factors are not the same from 12-tuple to 12-tuple either. The gain factors result in the following relationship for the probability density function of  $y_{chan}(l)$ :

$$f(y_{chan}(n)) = f(y_{chan}(n + 4P)) . \tag{28}$$

$P$  in (28) is an integer value. As a result, the distribution is not always of  $y_{chan}(l)$  due to one 12-tuple may be different from another 12-tuple.

If  $y_{chan}(l)$  is represented as the aggregation of the outputs of each 12-tuple, i.e.  $\{y_{chan}(l)\} = \{y_{chan}^1(l), y_{chan}^2(l), y_{chan}^3(l), y_{chan}^4(l)\}$  where the index  $k$  in  $y_{chan}^k(l)$  denotes the corresponding 12-tuple, a representation for the pdf of each 12-tuple filter output may be derived. This pdf is based on two subsets of coefficients of the 12-tuple: significant coefficients, and the other “smaller” coefficients. The former subset provides an antipodal distribution, while the latter subset may provide more of a Gaussian distribution. “Significant” in this case can be specified as a coefficient that differs in gain from the next highest gain coefficient by a pre-specified amount. For instance, the 12-tuple depicted in Figure 3 has one significant coefficient (assuming that a 16 dB margin defines significance). However, the 12-tuple of Figure 4 does not seem to have significant coefficients, based on a 16 dB margin. A general form for the pdf of  $y_{chan}^k(l)$  based on a particular 12-tuple is

$$f(y_{chan}^k(l)) = f(\{h^k\}, x_{chan}) , \tag{29}$$

where  $\{h^k\}$  are the filter coefficients corresponding to 12-tuple  $k$  and  $x_{chan}$  represents the input chips. If only one of the coefficients is significant for the 12-tuple is significant, and the other

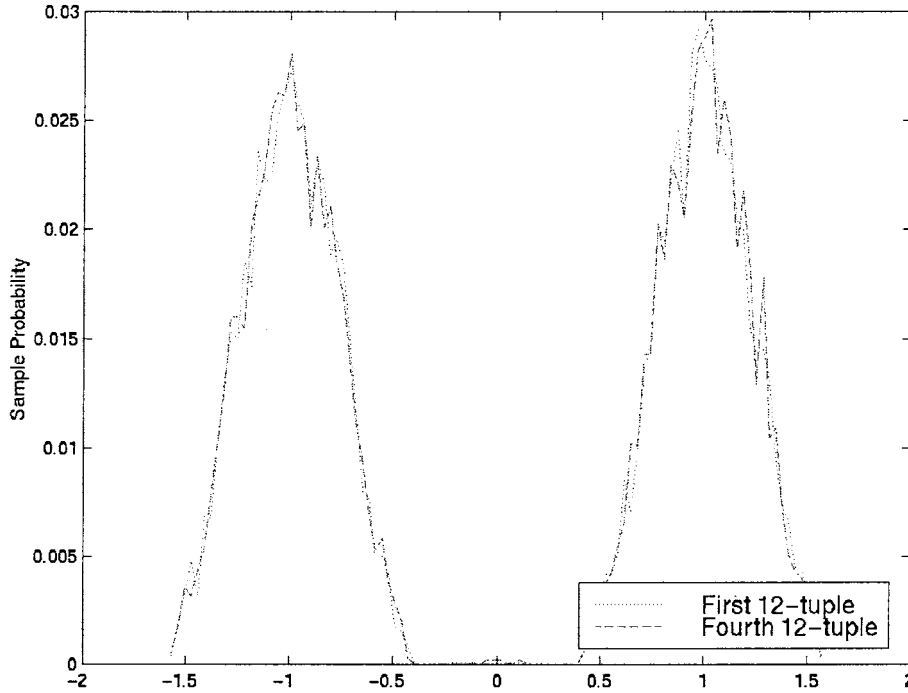


Figure 7. Sample distributions of  $h^1$  and  $h^4$ .

coefficients are very close to one another, then the distribution resembles an antipodal signal in white noise:

$$f(y_{chan}^k(l)) = \frac{1}{2} \frac{1}{\sqrt{2\pi}\sigma^2} e^{-\frac{(x-1)^2}{2\sigma^2}} + \frac{1}{2} \frac{1}{\sqrt{2\pi}\sigma^2} e^{-\frac{(x+1)^2}{2\sigma^2}}. \quad (30)$$

This distribution is evident in the 12-tuples  $h^1$  and  $h^4$ , as can be seen in the sample distributions given in Figure 7. The variance  $\sigma^2$  of the additive Gaussian noise, as shown in (30), can be found by the following relationship:  $\sigma^2 = E\{(y_{chan}^k(l))^2\} - 1$ .

However, the distribution for the other two 12-tuples comes about from coefficient sets in which no coefficient is really significant. One would assume that such a scenario would create a Gaussian distribution, as most of the coefficients would be close to one another. However, the range of the coefficients in each of the 12-tuples  $h^2$  and  $h^3$  is nearly 30 dB, meaning that the coefficients are not similar in value. As a result, these two distributions result from the weighted sum of IID binary random variables; this distribution cannot be approximated as Gaussian. Sample distributions are shown in Figure 8.

#### 4.1. NOTE: STAIRSTEP FILTER

As stated in Section 2, the problem of nonstationarity could be remedied by using a “stairstep”-shaped filter. Recall that given the oversampling factor for the filter,  $O$  ( $O = 4$  for cdma2000), and a filter length  $R \times O$ , the requirement for the causal form of such a filter would be:

$$h_O(r) = h_O(r+1) = h_O(r+2) = \dots = h_O(r+O-1) \quad (31)$$

$$r = 0, O, 2O, \dots, R \times O.$$

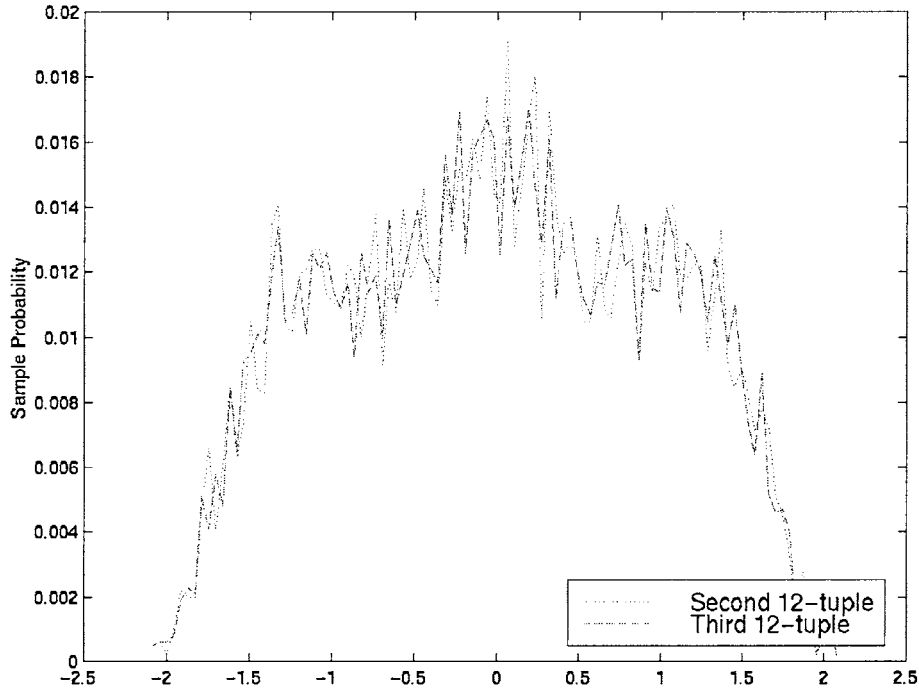


Figure 8. Sample distributions of  $h^2$  and  $h^3$ .

The constraint of (31) is extremely limiting. As a result, one may not be able to design a stairstep filter to meet necessary spectral requirements. A stairstep filter using the  $0.2 \mu\text{s}$  tap-spacing of the cdma2000 baseband filter is shown in Figure 9.

#### 4.2. OPTIMAL QUANTIZATION

In the analysis to follow, only one code channel is considered for simplicity's sake. Assume as in Section 3, the DAC takes as input zero-mean data, denoted by  $x$ , and given the DAC outputs  $L$  discrete levels spaced  $\Delta$  apart, the DAC output is taken from the discrete levels  $\{-(L-1)\Delta/2, \dots, -\Delta/2, \Delta/2, \dots, (L-1)\Delta/2\}$ . If  $x$  is a cdma2000 transmitted signal, such as  $y_{chan}$ , then the function  $p_x(x, i)$  is not continuous over  $i$ . As shown previously in Figures 7 and 8, for the cdma2000 signal  $y_{chan}$  only two pdf's exist. If these two pdf's are denoted as  $p_x(x, 1)$  and  $p_x(x, 2)$ , then the mean-squared error may now be written as

$$\begin{aligned}
 E\{(r-x)^2\} &= \sum_{k=1}^{\frac{L}{2}-1} \int_{(k-1)\Delta}^{k\Delta} \left(x - \frac{(2k-1)\Delta}{2}\right)^2 p_x(x, 1) dx \\
 &+ \int_{\frac{L\Delta}{2}}^{\infty} \left(x - \frac{(L-1)\Delta}{2}\right)^2 p_x(x, 1) dx \\
 &+ \sum_{k=1}^{\frac{L}{2}-1} \int_{(k-1)\Delta}^{k\Delta} \left(x - \frac{(2k-1)\Delta}{2}\right)^2 p_x(x, 2) dx \\
 &+ \int_{\frac{L\Delta}{2}}^{\infty} \left(x - \frac{(L-1)\Delta}{2}\right)^2 p_x(x, 2) dx.
 \end{aligned} \tag{32}$$

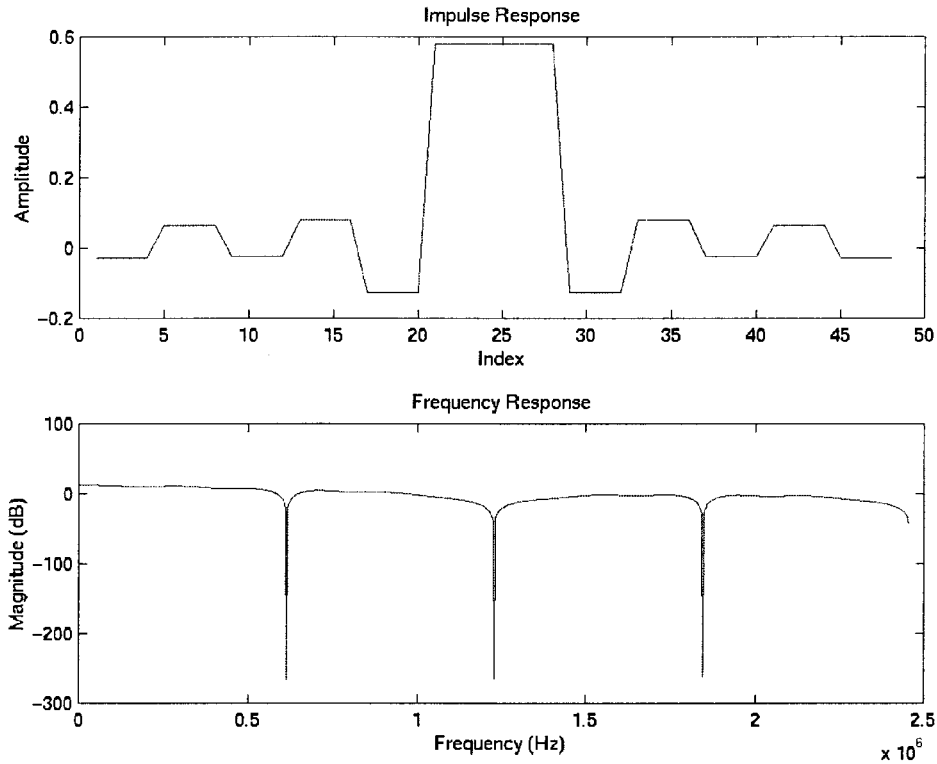


Figure 9. Stairstep filter.

Simple data passed through the baseband pulse-shaping filter, scaled, and quantized assuming 8 bits of quantization were available. The results are graphed for different scaling factors in Figure 10 (in dB-dB scale).

Optimal scaling is provided for the two pdf's present in a cdma2000 reverse link channel in Figure 11.

To further examine the effect of spectral distortion, assume that for the cdma2000 signal, there are two positive scaling factors being used, denoted as  $k_1$  and  $k_2$ . Let us represent the scaling factors as simply a square wave defined as

$$k(l) = \begin{cases} k_1, & l = \dots, -8, -7, -4, -3, 0, 1, 4, 5, 8, 9, 12, 13, \dots \\ k_2, & l = \dots, -6, -5, -2, -1, 2, 3, 6, 7, 10, 11, 14, 15, \dots \end{cases} \quad (33)$$

Let us define a square function  $t(l)$  as

$$t(l) = \text{sgn}(\cos(l)). \quad (34)$$

Then the following may be derived:

$$k(l) = (t(l) + 1) \left| \frac{k_2 - k_1}{2} \right| + (\min(k_1, k_2)). \quad (35)$$

Remembering that a square function may be written in terms of its Fourier series as a sum of sinusoids, we can redefine  $t(l)$  as

$$t(l) = \sum_{i=0}^{\infty} \frac{(-1)^i}{2i+1} \cos\left(\frac{\pi}{2}(2i+1)l\right). \quad (36)$$

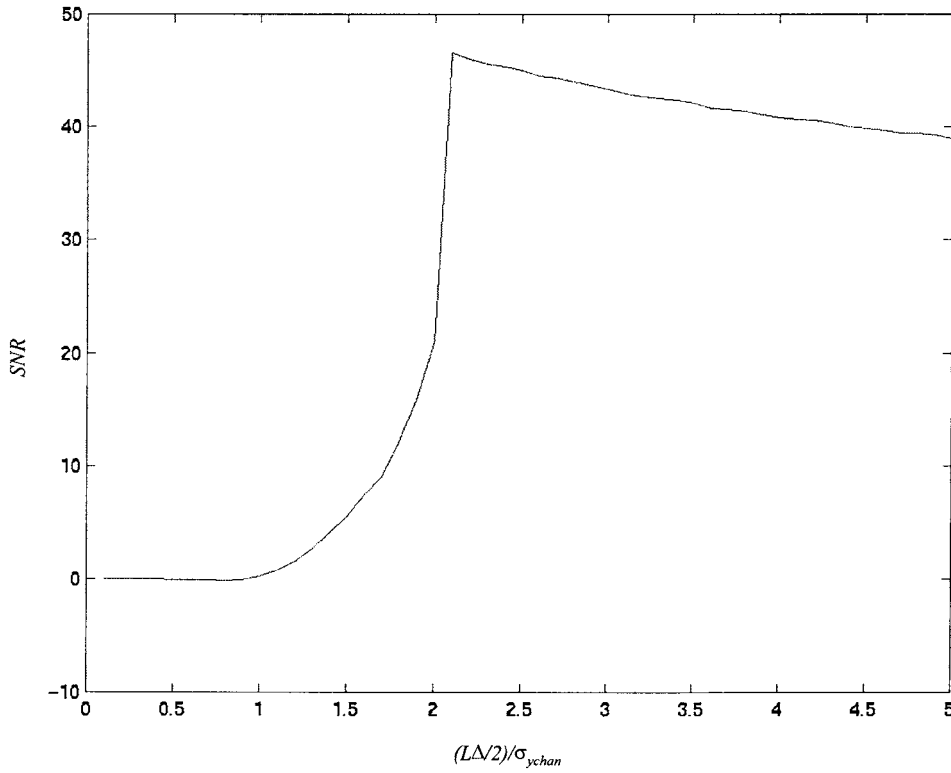


Figure 10. Optimal scaling.

The discrete-time Fourier transform of  $t(l)$  is given by [9]

$$T(e^{j\omega}) = \sum_{i=0}^{\infty} \frac{\pi(-1)^i}{2i+1} \sum_{k=-\infty}^{\infty} \begin{bmatrix} \delta\left(\omega - \frac{\pi}{2}(2i+1) + 2\pi k\right) \\ + \delta\left(\omega + \frac{\pi}{2}(2i+1) + 2\pi k\right) \end{bmatrix}. \quad (37)$$

The discrete-time Fourier transform of  $k(l)$  may now be found in terms of the discrete-time Fourier transform of  $t(l)$  as

$$K(e^{j\omega}) = \left| \frac{k_2 - k_1}{2} \right| T(e^{j\omega}) + \left( \left| \frac{k_2 - k_1}{2} \right| + \min(k_1, k_2) \right) \sum_{k=-\infty}^{\infty} 2\pi \delta(\omega + 2\pi k). \quad (38)$$

In (38), the second term in the sum is essentially a DC-offset term. The leftover square wave has a spectral response with the fundamental frequency centered at the chipping frequency.

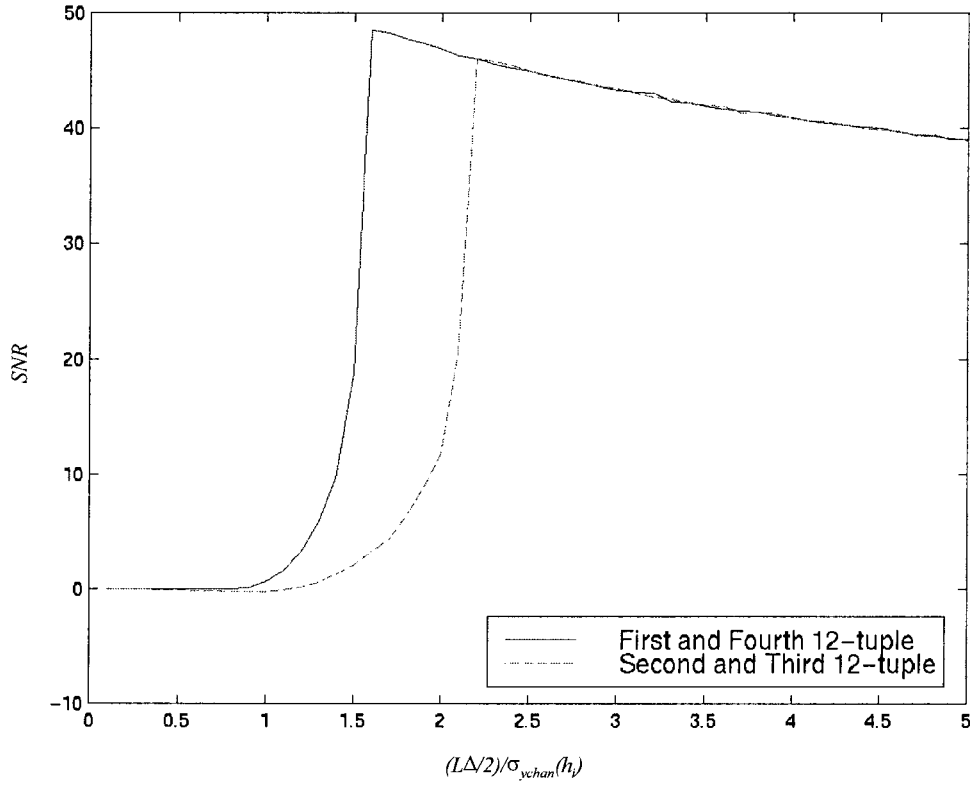


Figure 11. Optimal scaling as a function of 12-tuples.

Multiplying this scaling signal by  $y_{chan}(l)$  will result in a convolution of the spectral responses of the two signals. Therefore, the resultant spectrum of  $y_{chan}(l)$  is

$$\begin{aligned}
 K(e^{j\omega} * Y_{chan}(e^{j\omega})) = & \left| \frac{k_2 - k_1}{2} \right| \sum_{i=0}^{\infty} \frac{\pi(-1)^i}{2i+1} \sum_{k=-\infty}^{\infty} \left[ \begin{array}{l} Y_{chan}\left(e^{j(\omega - \frac{\pi}{2}(2i+1) + 2\pi k)}\right) \\ + Y_{chan}\left(e^{j(\omega - \frac{\pi}{2}(2i+1) + 2\pi k)}\right) \end{array} \right] \\
 & + \left( \left| \frac{k_2 - k_1}{2} \right| + \min(k_1, k_2) \right) \sum_{k=-\infty}^{\infty} 2\pi Y_{chan}(e^{j(\omega + 2\pi k)}).
 \end{aligned} \quad (39)$$

Since  $y_{chan}(l)$  is bandlimited to half of the chipping frequency, then the spectrum after adaptive scaling could reach as high as  $1\frac{1}{2}$  times the chipping frequency, due to the first term in (39). In addition, higher-order spectral products resulting from the odd harmonics of  $k(l)$  also result in spectral distortion. The second term in (39) results in a DC-offset. However, as  $k_1$  and  $k_2$  move closer together in value, the more  $k(l)$  resembles a constant, which results in no spectral modification of  $y_{chan}(l)$ . This can be seen by examining (35), which leads to

$$\lim_{k_1 \rightarrow k_2} k(l) = k_1 = k_2. \quad (40)$$

As a result, the following spectrum results

$$\begin{aligned} \lim_{k_1 \rightarrow k_2} K(e^{j\omega}) * Y_{chan}(e^{j\omega}) &= k_1 \sum_{k=-\infty}^{\infty} 2\pi Y_{chan}(e^{j(\omega+2\pi k)}) \\ &= k_2 \sum_{k=-\infty}^{\infty} 2\pi Y_{chan}(e^{j(\omega+2\pi k)}). \end{aligned} \quad (41)$$

Thus, if the optimal scaling factor is different for the different distributions, an adaptive quantization algorithm may result in significant spectral growth; there exists a tradeoff between spectral growth and quantization noise. One may try and “undo” the adaptive scaling at the output of the D/A converter (which results in an inversion of  $k(l)$ ), but this would require rapidly switching amplification in the analog domain, which adds a degree of complexity to transceiver design.

“Undoing” the spectral distortion after D/A conversion involves rescaling the data. This involves simply multiplying the converted signal by  $1/k(l)$ . Additional amplification may be needed if the rescaling operation results in a deviation from the desired output power.

The quantization noise may be derived from either Figure 10 or Figure 11, depending on the type of quantization scheme used. It should be noted that all previous quantization analysis was performed with respect to one channel; if the signal results from aggregating and scaling channels, then this quantization analysis is not optimal. However, based on a fixed-gain scenario, an optimal quantization characteristic may be found.

#### 4.3. CHANNEL AGGREGATION

In the case of channel aggregation, the optimal quantizers derived above will change. This is due to the fact that the distributions of the data after channel aggregation, although cyclostationary, will vary with the number of channels and the channel scaling. However, one may use the exact same methodology for deriving a fixed-scaling or adaptive-scaling quantizer, given a scenario for channel aggregation.

The modulation for the reverse link of cdma2000, as pictured in Figure 1, will still result in 4 distinct distributions from each baseband filter on I and on Q.

### 5. Example: IS-136 Signal Modeling Prior to Digital-to-Analog Conversion

The IS-136 TDMA system is widely deployed in North America and must meet electromagnetic compatibility constraints with a wide variety of consumer electronics equipment. Therefore, similar to cdma2000, design constraints exist for IS-136 in terms of emissions. The IS-136 system, being a pulse-shaped system, is sensitive to the restricted dynamic range of typical transceivers.

Of primary interest is the IS-136 uplink transmitter. A typical transmitter is shown in Figure 12 [10].

In Figure 12, the slot data is the user traffic for its time slot (there are 6 slots per 40 ms period). In addition, the combination of the serial-to-parallel converter and the differential

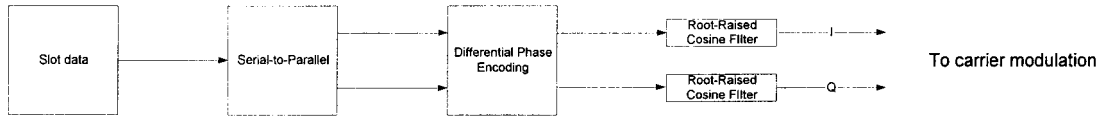


Figure 12. IS-136 baseband transmitter.

phase encoding constitute a  $\pi/4$ -DQPSK (differential QPSK) modulation. Finally, the root-raised cosine filter may be defined by its impulse response:

$$h(n) = \sqrt{\frac{\sin\left(\frac{\pi n}{N}\right) \cos\left(\frac{\alpha \pi n}{N}\right)}{\frac{\pi n}{N} \left(1 - 4\alpha^2 \frac{n^2}{N^2}\right)}}. \quad (42)$$

In (42),  $n$  is the discrete-time index,  $N$  is the symbol period with respect to  $n$ , and  $\alpha$  is the “rolloff factor” (0.35 in IS-136). The raised-cosine filter is normally implemented as a finite impulse-response (FIR) filter, which means that the one is primarily interested in the truncated response of (42). This type of filter satisfies the “zero-ISI” criterion: i.e. the zero-crossings of the impulse response fall on multiples of the symbol period. In addition, each slot of user traffic is formatted such that the user traffic rate is effectively 48.3 kbps.

The  $\pi/4$ -DQPSK modulation results in a constellation whose 8 symbols are placed on the unit circle at 45-degree intervals. Assuming the “first” symbol in this constellation is at ( $I = 1, Q = 0$ ), then one may assume that the symbols to be transmitted on I or Q prior to pulse-shaping may be drawn from the alphabet  $\{-1, -1/\sqrt{2}, 0, 1/\sqrt{2}, 1\}$ , with respective probabilities  $\{1/8, 2/8, 2/8, 2/8, 1/8\}$ . This differs from the previous cdma2000 example of Section 4, where all members of the source alphabet were equiprobable. Nevertheless, the generating process may be assumed to be stationary. The IS-136 constellation is shown in Figure 13.

The raised-cosine filter is normally implemented digitally, and as with cdma2000 normally acts as an interpolating filter. Some implementations assume 194.4 kHz spacing (for instance, in [11]), which corresponds to an upsampling factor of 4; while other implementations require even higher rates of upsampling (for instance, 777.6 kHz in [12]). For the sake of analysis, an upsampling ratio of 4 with a truncation length of 25 will be considered for the raised-cosine filter from herein:

$$h(n) = \sqrt{\frac{\sin\left(\frac{\pi n}{4}\right) \cos\left(\frac{0.35\pi n}{4}\right)}{\frac{\pi n}{4} \left(1 - 4(0.35)^2 \frac{n^2}{4^2}\right)}} \quad 0 \leq n < 25. \quad (43)$$

If the symbols after differential coding may be represented once again as  $d_{chan}(l)$  where  $chan$  refers to either I or Q, then the filter output may be written as

$$y_{chan}(l) = \sum_{i=0}^{24} h(i) d_{chan}(l-i). \quad (44)$$

This signal is cyclostationary, and its pdf satisfies the relationship:

$$f(y_{chan}(n)) = f(y_{chan}(n + 4P)), \quad (45)$$

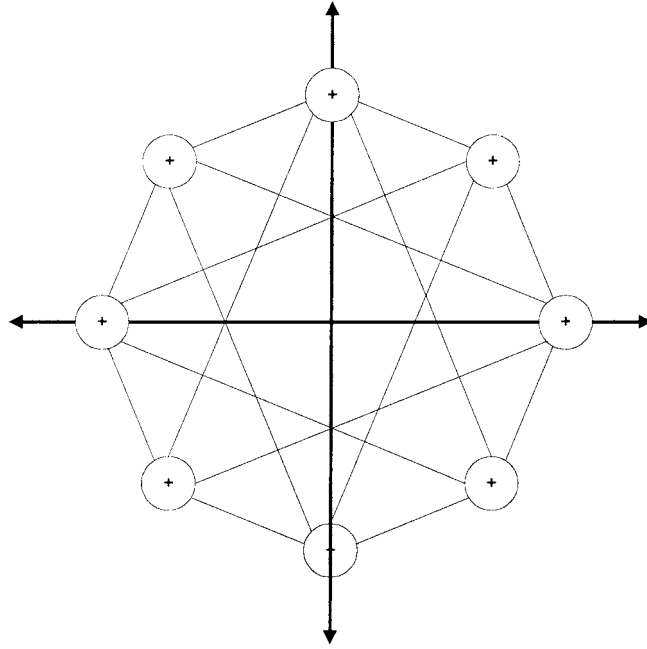


Figure 13. IS-136 constellation.

where  $P$  is an arbitrary integer. Recalling from Section 4 that the filter length  $N$  may be represented as  $N = \text{floor}(N/L) + R$ , then clearly  $L = 4$  and  $R = 1$  in the case of the 25-tap filter with oversampling factor of 4. As per the analysis of Section 2, since the number of filter coefficients  $N = 25$  is not an integer multiple of the upsampling factor 4, as many as three pdf's exist. The 25 coefficients may be divided into subsets as

$$\begin{aligned} h^i &= \{h(i), h(4+i), \dots, h((\text{ceil}(25/4) - 1)4 + i)\}, & 0 \leq i < 1 \\ h^i &= \{h(i), h(4+i), \dots, h((\text{floor}(25/4) - 1)4 + i)\}, & 1 \leq i < 4. \end{aligned} \quad (46)$$

As predicted by the analysis of Section 4 (see (19)), the pdf corresponding to  $h^1$  should be equal to the pdf corresponding to  $h^3$ . This can be seen in the histograms of the output of each 13- and 12-tuple, as shown in Figure 14.

Observing Figure 14, as predicted the 2nd and 4th 12-tuples show similar pdf's.

### 5.1. OPTIMAL QUANTIZATION

The optimal quantization procedure should be identical to what was presented in Section 4.2. However, optimal scaling coefficients for three pdf's must now be found. We start from the assumptions of Section 4.2: (1) The DAC takes as input zero-mean data, denoted by  $x$ , (2) Given the DAC outputs  $L$  discrete levels spaced  $\Delta$  apart, the DAC output is taken from the discrete levels  $\{-(L-1)\Delta/2, \dots, -\Delta/2, \Delta/2, \dots, (L-1)\Delta/2\}$ , (3) The input signal is divided into intervals as  $x \in \{(-\infty, -L\Delta/2], (-L\Delta/2, -(L+2)\Delta/2], \dots, ((L-2)\Delta/2, L\Delta/2], (L\Delta/2, \infty)\}$ , (4) Each of the DAC output levels  $\{-(L-1)\Delta/2, \dots, -\Delta/2, \Delta/2, \dots, (L-1)\Delta/2\}$  correspond to the input intervals  $\{(-L\Delta/2, -(L+2)\Delta/2], \dots, ((L-2)\Delta/2, L\Delta/2]\}$ , and (5) The DAC rail output levels,  $\{-(L-1)\Delta/2, (L-1)\Delta/2\}$ , correspond to the input intervals  $\{(-\infty, -L\Delta/2], (L\Delta/2, \infty)\}$ . We will assume an

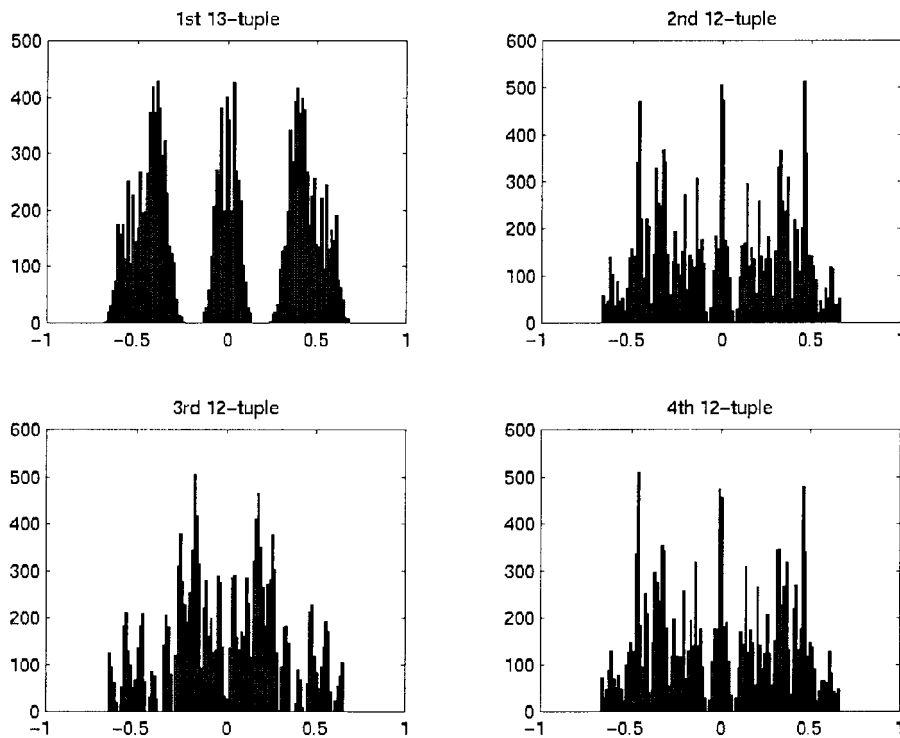


Figure 14. Sample histograms for IS-136 root-raised cosine filter.

8-bit DAC is being used (as in [12]), and we can derive the optimal fixed quantization scaling by examining the SNR as a function of the scaling coefficient with respect to the input signal variance, as shown in Figure 15 (dB-dB scale).

The scaling as a function of  $n$ -tuple pdf's is shown in Figure 16 (dB-dB scale).

The peak SNR for the fixed quantization (optimized over the entire pdf of the signal) is 45.9 dB, while the mean peak SNR for the adaptive quantization method (optimized for the instantaneous pdf) is 46.24 dB.

For comparison, similar analysis (not pictured) for 10-bit quantization methods shows a peak SNR of 57.98 dB for fixed quantization and 58.81 dB for adaptive quantization.

## 6. Digital-to-Analog Conversion Modeling

The two main nonidealities that affect D/A converters are integral nonlinearity (INL) and differential nonlinearity (DNL). If one thinks of the D/A converter output levels versus the corresponding input binary codes and then draws a curve through these output levels, then INL denotes the maximum deviation of this curve from a straight line of unity slope. DNL refers to the maximum deviation of the spacing of the output DAC levels from the ideal spacing of one least-significant bit (LSB). Both quantities are usually expressed in LSB's. The concept of INL is shown in Figure 17.

The deviation from the linear mapping increases quantization noise; however, A/D converters may be difficult to design if the INL requirements are very small (much less than 1 bit for most typical converters). An illustration of quarter-bit DNL is shown in Figure 18.

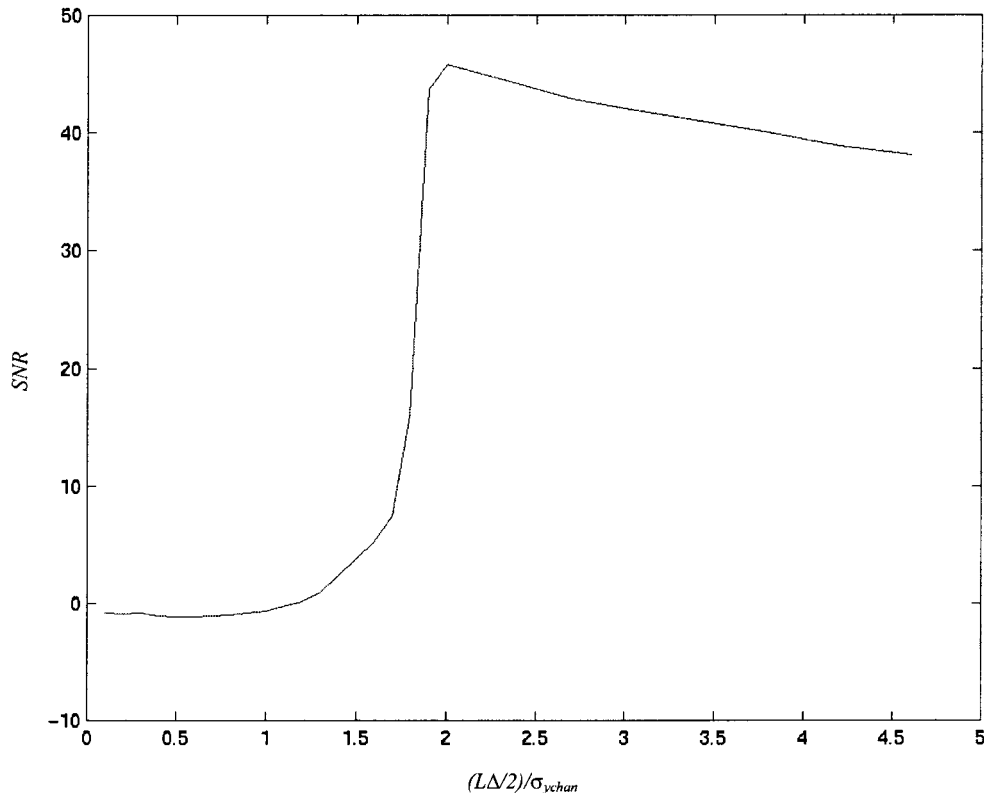


Figure 15. IS-136 8-bit fixed-quantization optimal scaling.

## 7. Simulations

Simulations using behavioral modeling of both cdma2000 and IS-136 transmitters were performed. Comparisons of fixed quantization and adaptive quantization methods are given in this section.

### 7.1. CDMA2000 SIMULATIONS

An adaptive scaling method was compared to the fixed-scaling method in a simulation of a cdma2000 transmitter at transmitting a signal of 1.25 MHz bandwidth. The handset transmitter block diagram is given in Figure 19 for the fixed quantization method. The adaptive quantization method required a re-scaling operation at the output of the D/A converters. This was simulated as an adaptive gain factor integrated into the low-pass filters following the DAC's, as shown in Figure 20.

Both methods were simulated assuming 8-bit DAC's (2 LSB's INL, 0.9 LSB's DNL) followed by a 3rd-order Butterworth low-pass filter (630 kHz corner frequency) and IQ-modulator. The IQ-modulator in turn was fed into a transmit AGC amplifier. The output of the AGC amplifier went into an image-rejecting upconverter, which brought the signal from IF to carrier. Finally, the upconverter output went into a power amplifier. All of these basic components were simulated using behavioral models. The IQ-modulator was simulated to have 20 dB of carrier suppression. The upconverter was simulated to have 25 dB LO-to-RF isolation and 33 dB IF-to-RF isolation. The transmit AGC amplifier was simulated at 28 dB

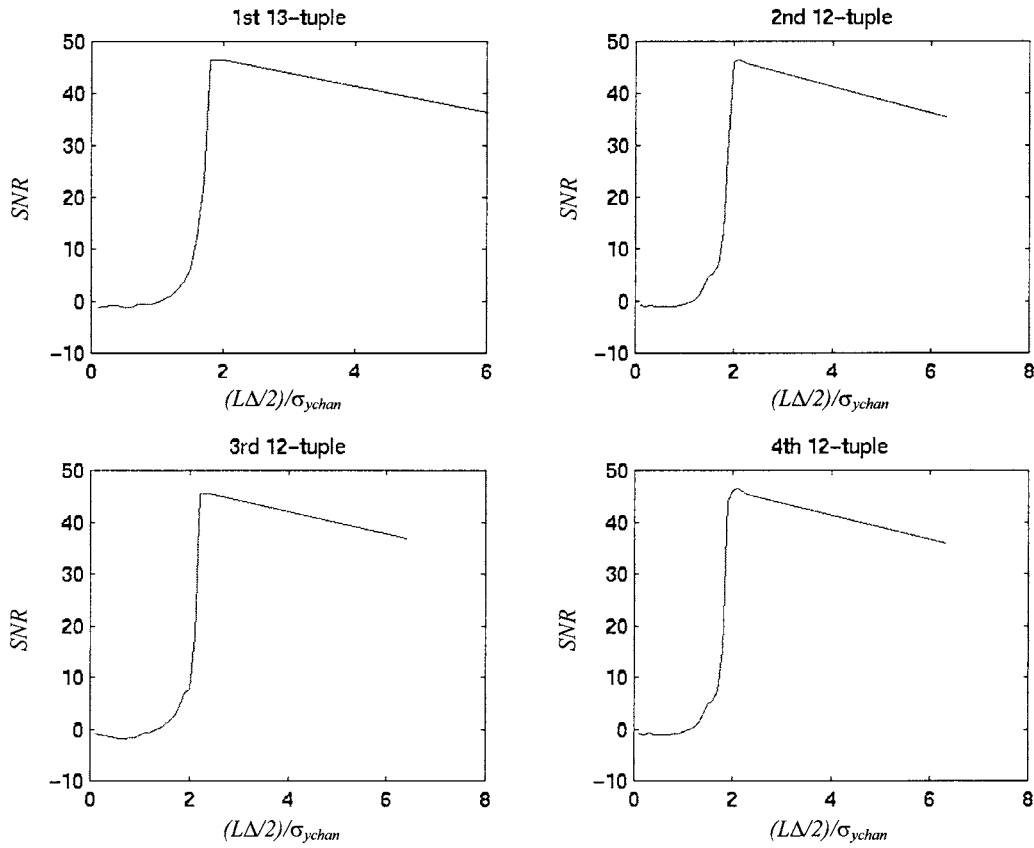


Figure 16. Adaptive 8-bit scaling.

gain and  $-15$  dBm input IP3. Finally, the PA was simulated to compress at input powers greater than 5 dBm, using a typical AM-to-AM and AM-to-PM response to a single-tone [13].

Results were analyzed in terms of emissions and waveform quality [14]. In order to define waveform quality, one starts out with the ideal transmitted signal. The ideal signal envelope,  $R(t)$ , is defined as

$$\begin{aligned}
 R(kT_s) = & \sum_n [h(kT_s - nT_c) \cos(\phi_n)] \\
 & + j \sum_n \left[ h \left( kT_s - nT_c - \frac{T_c}{2} \right) \sin(\phi_n) \right],
 \end{aligned} \tag{47}$$

where  $T_s$  is the sampling period,  $k$  the sample index,  $h(t)$  is the baseband pulse shaping filter, and  $\phi_n$  is the phase of the  $n$ th chip. Therefore, given the ideal transmitter frequency of  $\omega_0$ , the ideal signal at the antenna connector would be

$$s(t) = R(t)e^{-j\omega_0 t}. \tag{48}$$

The actual transmitted waveform may be written in terms of the ideal signal waveform as

$$x(t) = C[R(t + \tau) + E(t)]e^{-j(\omega_0 + \Delta\omega)(t + \tau)}, \tag{49}$$

where  $\tau$  is the time offset of the actual signal versus the ideal signal,  $\Delta\omega$  is the frequency offset from the ideal transmitter frequency, and  $C$  represents a complex scaling factor, and

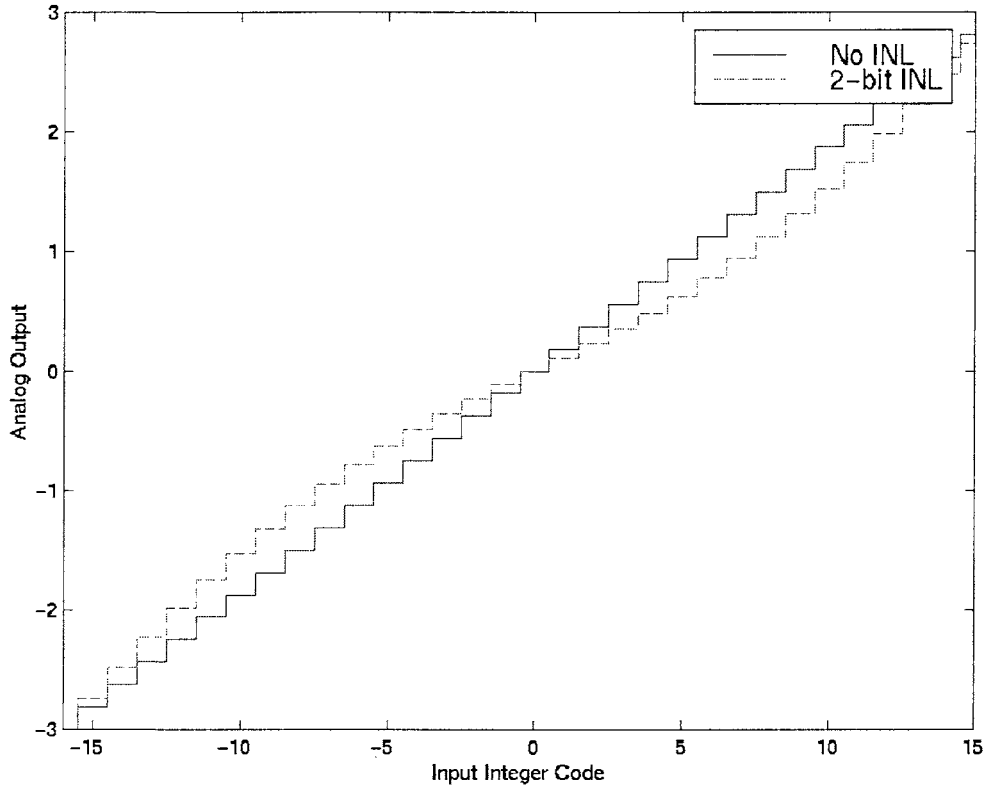


Figure 17. Integral nonlinearity for 5-bit DAC.

$E(t)$  is the complex envelope error. The frequency error must be less than 150 Hz. In order to measure the waveform quality, the frequency and time error must be estimated and corrected. This compensated waveform, whose envelope is  $Z(t)$ , will be sampled every  $T_s$  seconds to form the waveform quality

$$\rho = \frac{\left| \sum_{k=1}^M R_k Z_k^* \right|^2}{\sum_{k=1}^M |R_k|^2 \sum_{k=1}^M |Z_k|^2}, \quad (50)$$

where  $M$  is the number of samples (at least 1229, or 0.5 ms) and  $R_k$  and  $Z_k$  are discrete half-chip spaced samples of  $R(t)$  and  $Z(t)$  respectively. Emissions are calculated as the ratio of the maximum power emitted in any 30 kHz band at a minimum frequency offset from the center frequency of the signal at the antenna connector to the total power emitted in the 1.25 MHz signal bandwidth; emissions are usually provided in units of dBc's. For these simulations, the 1.25 and 2.5 MHz offsets emissions are calculated.

Only a single channel transmission (pilot channel) was simulated over 30 trials of 0.5 ms each. The baseband filter was simulated using floating-point coefficients. Based on the results given in Figures 10 and 11, scaling factors were chosen to optimize SNR of resultant DAC signal. In order to minimize spectral distortion for the adaptive quantization, an inversion of the scaling was applied at the output of the DAC. 10 trials of 1024 chips were performed for

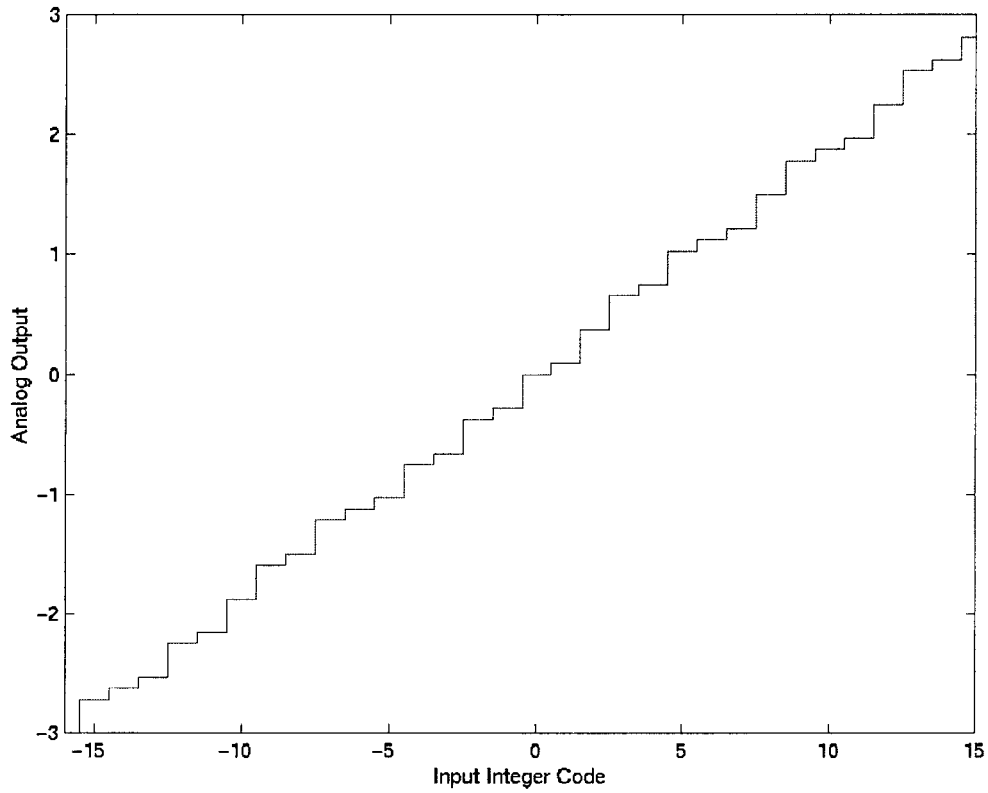


Figure 18.  $1/2$ -bit DNL for 5-bit DAC.

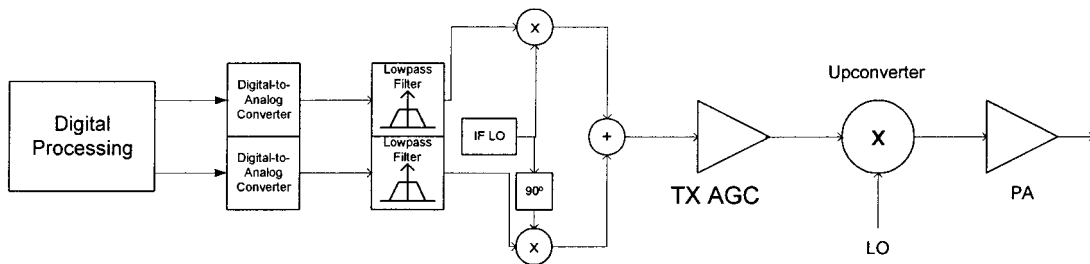


Figure 19. CDMA transmitter.

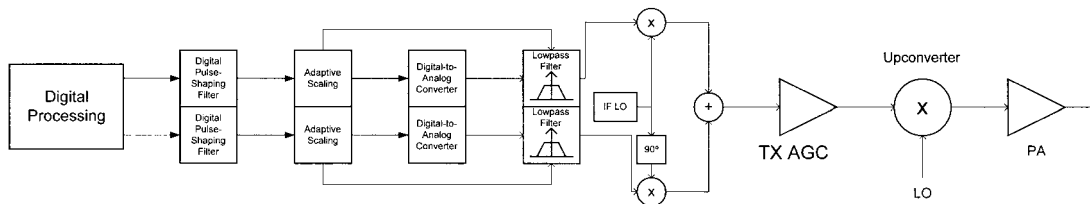


Figure 20. CDMA transmitter with adaptive scaling.

each type of quantization scheme at 6 dB PA backoff. The emissions at 1.25 and 2.5 MHz for the adaptive quantization algorithm were  $-58.7$  and  $-76.9$  dBc, respectively (the standard deviations for these two measurements were 1.33 and 6.79 dB, respectively). For the fixed quantization algorithm, the emissions at 1.25 and 2.5 MHz were  $-57.1$  and  $-70.5$  dBc (the standard deviations were 1.18 and 2.52 dB). The waveform quality for the adaptive quantizer was 0.9693 (standard deviation 0.0019) and for the fixed quantizer was 0.9698 (standard deviation 0.0019). The adaptive quantizer provided no performance advantage over the fixed quantizer in terms of waveform quality, but provided smaller emissions. The most likely reason for improved emissions performance of the adaptive quantizer was due to the reduction in quantization noise, which is usually modeled as wideband.

#### 7.1.1. *cdma2000 Simulations: Channel Aggregation Case*

It is of interest to examine the performance of the adaptive scaling method versus the fixed scaling method for the case of channel aggregation. The case which was examined was the case of pilot and fundamental channel transmission, with the relative channel-to-pilot gain  $G_f$  being 2 (this ratio is robust for a large number cases; for a more rigorous study see [15]). After 10 trials of 1024 chips under the same simulation conditions as before, the emissions at 1.25 and 2.5 MHz for the adaptive quantization algorithm were  $-57.0$  and  $-75.4$  dBc, respectively (the standard deviations for these two measurements were 1.47 and 3.43 dB, respectively). For the fixed quantization algorithm, the emissions at 1.25 and 2.5 MHz were  $-56.4$  and  $-74.8$  dBc (the standard deviations were 1.41 and 3.22 dB). The waveform quality for the adaptive quantizer was 0.9659 (standard deviation 0.0013) and for the fixed quantizer was 0.9670 (standard deviation 0.0014). Once again, the adaptive quantizer provided no performance advantage over the fixed quantizer in terms of waveform quality, but provided smaller emissions.

## 7.2. IS-136 SIMULATIONS

The IS-136 uplink transmitter was simulated at baseband only. A top-level view of the simulated transmitter for the fixed quantization method is shown in Figure 21.

The root-raised cosine filter was a 25-tap version truncated version whose tap-spacing was at  $1/4$  of the symbol duration. The DAC's were perfectly linear 8-bit DAC's, and were followed by 4th-order lowpass Butterworth filters whose cutoff was at 70 kHz. The cutoff frequency for the lowpass filters was derived by simulation, and maximized the SNR of the transmitted signal. Using a simulation bandwidth of 80 times the symbol rate (3.888 MHz), the fixed quantization method was compared to the adaptive quantization method, which was implemented as pictured in Figure 22.

The mean SNR after 120 slots of test data for the adaptive quantization method (as measured after the lowpass filter) was 29.9544 dB, while for the same test data set the fixed quantization method yielded 29.6938 dB – a performance difference of 0.26 dB. This is close to the 0.34 dB performance difference derived from the analysis of Section 5.1.

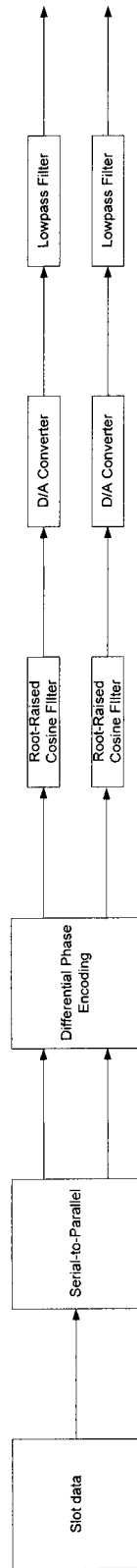


Figure 21. IS-135 baseband uplink transmitter.

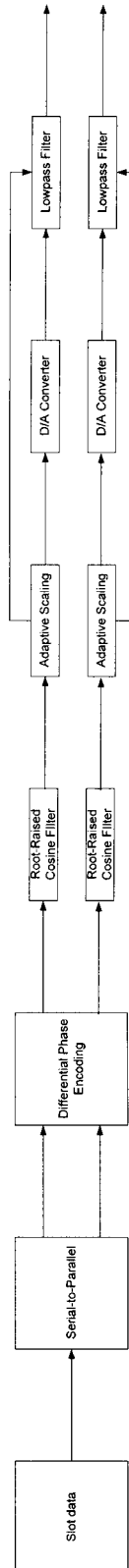


Figure 22. IS-136 baseband uplink transmitter with adaptive quantization.

## 8. Conclusions

Fixed and adaptive quantization algorithms were derived with respect to proper scaling and truncation prior to D/A conversion for pulse amplitude modulated systems. These algorithms were simulated using typical parameters for CDMA and transmitters. In particular, the cdma2000 reverse link and IS-136 uplink transmitters were analyzed with respect to digital-to-analog conversion. For the cdma2000 system, simulations demonstrated that the adaptive quantization algorithm provided no performance benefit over the fixed quantization algorithm in terms of waveform quality, but provided improvement in terms of emissions. For the IS-136 system, simulations showed an enhancement in terms of SNR at baseband after D/A conversion. This implies that despite the complexity in implementation of an adaptive algorithm, this approach can be of use when emissions margin is insufficient with the fixed quantization method.

This method of adaptive and/or nonadaptive quantization with respect to the cyclostationary pdf of a cdma2000 signal or an IS-136 signal may be extended to any pulse amplitude modulated system. Further work should examine applications in other communications systems that use PAM, regardless of whether such systems are wireless or wireline.

## References

1. W.A. Gardner, *Cyclostationarity in Communications and Signal Processing*, IEEE Press: New York, 1994.
2. S. Dennett, *The cdma2000 ITU-R RTT Candidate Submission*, Ver. 18, The Telecommunications Industry Association, 1998.
3. M. Nettles, M. Chang, G. McAllister, B. Nise, C. Perisco, K. Sahota and J. Tero, "Analog Baseband Processor for CDMA/FM Portable Cellular Telephones", in *IEEE International Solid-State Circuits Conference 1995*, February 1995, pp. 328–329.
4. G. Mandyam, "Analysis of Impact on Handset Transmitter Design of the High-Speed Data Requirements in the IS-95-B CDMA Wireless Standard", in *IEEE Radio and Wireless Conference*, August 1998, pp. 193–196.
5. *TIA/EIA-136*, The Telecommunications Industry Association, October 16, 1998.
6. J. Proakis, *Digital Communications*, 2nd edn, McGraw-Hill Inc.: New York, 1989.
7. N.S. Jayant and P. Noll, *Digital Coding of Waveforms: Principles and Applications to Speech and Video*, Prentice-Hall Inc.: Englewood Cliffs, NJ, 1984.
8. *TIA/EIA/IS-95-A: Mobile Station-Base Station Compatibility Standard for Dual-Mode Wideband Spread Spectrum Cellular System*, The Telecommunications Industry Association, 1995.
9. A.V. Oppenheim and R.W. Schaffer, *Discrete-Time Signal Processing*, Prentice-Hall Inc.: Englewood Cliffs, NJ, 1989.
10. *TIA/EIA-136-131: Digital Traffic Channel Layer 1*, The Telecommunications Industry Association, October 16, 1998.
11. N. Van Bavel, P.C. Maulik, K.S. Albright and X.-M. Gong, "An Analog/Digital Interface for Cellular Telephony", in *IEEE 1994 Custom Integrated Conference*, May 1-4, 1994, pp. 395–398.
12. V. Friedman, K.R. Lakshmi Kumar, D.L. Price, T.N. Le and J. Kumar, "A Baseband Processor for IS-54 Cellular Telephony", *IEEE Journal of Solid-State Circuits*, Vol. 31, No. 5, pp. 646–655, 1996.
13. W. Struble, F. McGrath, K. Harrington and P. Nagle, "Understanding Linearity in Wireless Communication Amplifiers", *IEEE Journal of Solid-State Circuits*, Vol. 32, No. 9, pp. 1310–1318, 1997.
14. *ANSI/J-STD-018: Recommended Minimum Performance Requirements for 1.8 to 2.0 GHz Code Division Multiple Access (CDMA) Personal Stations*, American National Standards Institute, 1996.
15. F. Ling, "Pilot Assisted Coherent DS-SS Reverse-Link Communications with Optimal Robust Channel Estimation", in *International Conference on Acoustics, Speech, and Signal Processing 1997*, April 21–24, 1997, pp. 263–266.



**Giridhar D. Mandyam** is the research manager of the Wireless Data Access Group at Nokia Research Center, Irving, Texas. He received the B.S.E.E. degree *Magna Cum Laude* from Southern Methodist University (Dallas, Texas) in 1989, the M.S.E.E. degree from the University of Southern California (Los Angeles, California) in 1993, and the Ph.D. degree in electrical engineering from the University of New Mexico (Albuquerque, New Mexico) in 1996. He has worked for several companies on wireless communications equipment, including Qualcomm and Texas Instruments. In 1998, he joined Nokia, where he has worked on standardization and implementation concepts for cdma2000, 1X-EV, and WCDMA. He has authored or co-authored over 40 journal and conference publications and four book chapters. He also holds four U.S. patents in the area of wireless communications technology.